

# VisMMOE: Exploiting Visual-Expert Affinity for Efficient Visual-Language MoE Offloading

Cheng Xu, Xiaofeng Hou\*, Jiacheng Liu, Chao Li\*  
Shanghai Jiao Tong University  
Minhang Qu, Shanghai, China

## Abstract

Large-scale vision-language mixture-of-experts (VL-MoE) models provide strong multimodal capability, but efficient deployment on memory-constrained platforms remains difficult. Existing MoE offloading systems are largely designed for text-centric workloads and become much less effective for visual-heavy inputs, where large numbers of visual tokens induce broader and less predictable expert accesses.

We present *VisMMOE*, a VL-MoE offloading system built on a single systems insight: pruning redundant visual tokens can improve offloading not only by reducing computation, but also by reshaping expert demand. We refer to this effect as *visual-expert affinity*: token pruning makes expert accesses more concentrated within layers and more stable across layers, producing a smaller and more predictable expert working set. Guided by this insight, *VisMMOE* combines affinity-aware token compression, lookahead expert prediction, and cache/pipeline orchestration to improve expert locality and prefetch effectiveness under tight memory budgets. We implement *VisMMOE* on multiple frameworks and evaluate it on representative VL-MoE models and benchmarks. *VisMMOE* improves end-to-end inference performance by up to 2.68 $\times$  and 1.61 $\times$ , respectively, over strong baselines for today's VL-MoE deployments while maintaining competitive accuracy.

**Keywords:** Multi-modal, Mixture-of-experts, Token compression, Expert cache, Prefetching

## ACM Reference Format:

Cheng Xu, Xiaofeng Hou\*, Jiacheng Liu, Chao Li\*. 2027. VisMMOE: Exploiting Visual-Expert Affinity for Efficient Visual-Language MoE Offloading. In *Proceedings of (ASPLOS 27)*. ACM, New York, NY, USA, 14 pages. <https://doi.org/XXXXXX.XXXXXX>

\*Corresponding authors.

Permission to make digital or hard copies of all or part of this work for personal or classroom use is granted without fee provided that copies are not made or distributed for profit or commercial advantage and that copies bear this notice and the full citation on the first page. Copyrights for components of this work owned by others than the author(s) must be honored. Abstracting with credit is permitted. To copy otherwise, or republish, to post on servers or to redistribute to lists, requires prior specific permission and/or a fee. Request permissions from [permissions@acm.org](mailto:permissions@acm.org). *ASPLOS 27, Woodstock, NY*

© 2027 Copyright held by the owner/author(s). Publication rights licensed to ACM.

ACM ISBN 978-1-4503-XXXX-X/2018/06  
<https://doi.org/XXXXXX.XXXXXX>

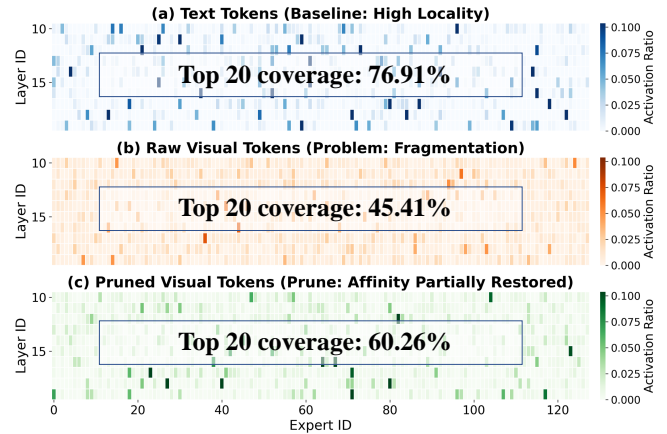


**Figure 1.** Expert activation distribution of Qwen3-VL-30B-A3B with 128 experts per layer. The x-axis is the expert ID, the y-axis is the layer ID, and darker color indicates a higher activation ratio. Text tokens exhibit strong locality, whereas raw visual tokens induce fragmented expert activations. After token pruning, the activation pattern becomes substantially more concentrated (+32% relative).

## 1 Introduction

Vision-Language Large Language Models (VL-LLMs) are rapidly becoming a default interface for interactive AI, where each request may combine text with a large number of visual tokens from high-resolution images [41, 45]. To scale model capacity without proportionally increasing per-token computation, many VL-LLMs adopt Mixture-of-Experts (MoE) [6, 34, 36, 51, 53], routing each token to only a small subset of experts. This sparsity makes MoE an attractive design point for large multimodal models such as MoE-LLaVA [25], DeepSeek-VL2 [42], and Qwen-VL-MoE [3]. Yet efficient single-GPU deployment remains challenging under tight memory budgets and latency constraints [9], where expert movement from host to GPU often dominates runtime.

In practice, memory-constrained deployment [8, 13, 36, 48, 51] often relies on *expert offloading*, keeping only a small working set of experts in GPU memory while fetching the rest on demand. Prior MoE systems [7, 40, 46] reduce swapping overhead through expert caching and predictive prefetching. These techniques [37, 50] are effective when expert accesses remain concentrated and predictable, but they are

substantially less effective for VL-MoEs. As shown in Figure 1, text tokens activate a relatively compact subset of experts, whereas raw visual tokens induce much more scattered expert activations across layers. This fragmentation directly hurts offloading efficiency: it reduces cache reuse, increases non-reusable transfers, and often leaves expert movement on the critical path. Importantly, Figure 1 also shows that this behavior is not inherent to visual inputs. After pruning redundant visual tokens, the activation pattern becomes noticeably more concentrated, partially restoring locality and predictability.

This observation points to a systems opportunity rooted in the redundancy of visual inputs. Unlike text sequences, visual inputs contain many low-information patches that contribute little to downstream reasoning but can still perturb router decisions and activate a broad set of experts. While prior visual token compression methods primarily target compute reduction, our profiling reveals an additional systems effect: pruning redundant visual tokens can reduce the effective expert working set and improve routing regularity. We refer to this empirical trend as **Visual-Expert Affinity**. In VL-MoE deployment, token compression can therefore serve not only as a FLOPs-reduction tool, but also as a systems mechanism for improving cache reuse and prefetchability. Exploiting this opportunity for efficient offloading, however, remains non-trivial.

**Challenge 1: token compression should be aligned with expert locality.** Standard visual token compression is designed to preserve semantic salience and reduce FLOPs [26, 43, 47], but offloading efficiency is governed by a different objective: the size and compactness of the expert working set. As a result, tokens retained solely for semantic importance can still activate a dispersed set of experts, limiting parameter-access consolidation and keeping transfer overhead high. The runtime must therefore jointly balance reasoning fidelity and expert working-set compactness under GPU-memory and PCIe-bandwidth constraints.

**Challenge 2: offloading efficiency depends on accurate multi-layer prediction.** Modern fine-grained MoEs substantially expand the routing search space. Compared with coarse-grained designs with 8–16 experts [16, 40], models such as Qwen-VL-MoE route over much larger expert pools (e.g., 128 experts) [3]. In this regime, inaccurate prediction becomes increasingly expensive: prefetching too many irrelevant experts wastes bandwidth, while missing required experts leaves transfers on the critical path. Effective VL-MoE offloading therefore requires not only early lookahead, but also sufficiently precise prediction of the sparse expert working set needed in subsequent layers.

To address these challenges, we present *VisMMOE*, a VL-MoE offloading system that explicitly exploits Visual-Expert

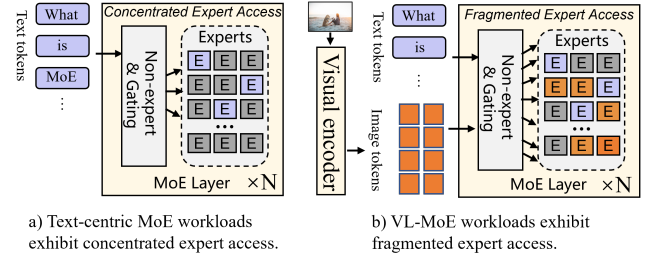


**Figure 2.** Why prior MoE offloading assumptions break for VL-MoEs: text-centric workloads induce concentrated expert access, whereas visual-heavy VL-MoE inputs broaden the effective expert working set.

*Affinity.* *VisMMOE* combines **Affinity-Aware Token Compressor** with **Compression-Guided Lookahead Predictor** to (i) prune redundant tokens while compacting the expert working set, and (ii) predict future expert demand early enough to enlarge the prefetch window. *VisMMOE* further introduces **Expert Caching and Pipeline Orchestrator** that jointly coordinates computation, I/O, and memory capacity, while overlapping compression and prediction overhead with expert transfers whenever possible. We implement *VisMMOE* on commodity GPU platforms and evaluate it on representative VL-MoE models. Our results show that *VisMMOE* substantially reduces end-to-end inference latency over strong practical baselines while maintaining competitive accuracy. In summary, this paper makes the following contributions:

- We identify a VL-specific offloading mismatch: compared with text-centric MoE workloads, raw visual inputs induce broader and less predictable expert accesses, weakening both cache reuse and lookahead-based prefetching.
- We show that visual token compression can serve as a systems mechanism for offloading, not merely a compute optimization: pruning redundant visual tokens improves expert locality and routing regularity.
- Guided by this insight, we design a compression-guided VL-MoE offloading system that combines token retention, expert prediction, and runtime cache/pipeline management to reduce exposed transfer overhead under tight memory budgets.
- We implement *VisMMOE* on commodity GPU platforms and evaluate it across representative VL-MoE models, runtimes, and hardware targets, demonstrating substantial end-to-end latency reductions over strong practical baselines.

The rest of the paper is organized as follows. Section 2 introduces the background and motivation. Section 3 presents the system design. Section 4 evaluates the system. Section 5 discusses related work, and Section 6 concludes.

**Table 1.** Analysis of Visual vs. Textual token distribution.

Dataset	Visual	User Text	Total Text <sup>†</sup>	Ratio (V/T)
MMBench	197	11	53	3.72×
MME	1107	18	60	<b>18.45×</b>
POPE	358	8	50	7.16×

<sup>†</sup>Includes a fixed 42-token system prompt overhead in this model.

## 2 Background and Motivation

### 2.1 VL-MoE Models and GPU Offloading

VL-MoE models combine a visual encoder with a Transformer language backbone whose feed-forward blocks are replaced by sparse MoE layers [3, 42, 44]. Similar to text-only MoE models, each token activates only a small subset of experts in each layer, reducing per-token computation while preserving large model capacity. However, the full expert pool remains too large to fit on a single GPU and must therefore be managed through expert offloading.

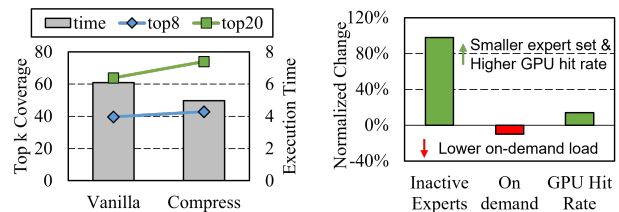
Existing MoE offloading systems [21, 24, 37, 40, 46] rely on a key assumption: expert accesses are sufficiently predictable that caching and prefetching can effectively hide data movement. This assumption is often reasonable in text-centric MoE workloads, where tokens repeatedly activate a compact subset of experts. As illustrated in Figure 2(a), such concentrated access leads to a small and reusable expert working set that is favorable for GPU caching and predictive prefetching.

VL-MoEs, however, operate in a different regime [14, 43]. In addition to text, each request may contain a large number of visual patch tokens produced by the visual encoder. These visual tokens induce broader and less regular routing behavior than text-centric workloads, expanding the expert working set and weakening routing predictability. As shown in Figure 2(b), VL-MoE requests therefore violate the locality assumptions that prior offloading strategies depend on.

### 2.2 Characterizing Raw VL-MoE Offloading

Expert movement is often the dominant bottleneck in memory-constrained MoE offloading. In our VL-MoE setting, even with predictive loading of 20 experts, CPU-GPU transfer still accounts for 62.1% and 86.9% of layer latency for Qwen3-VL and DeepSeek-VL2, respectively, indicating that expert movement frequently remains on the critical path (detailed in ??). However, VL-MoEs are challenging not merely because offloading is I/O-bound in general, but because visual-heavy inputs break the locality and predictability assumptions that prior MoE offloading systems rely on [37, 40, 46]. We characterize this mismatch from two complementary perspectives.

**Problem 1: Visual-heavy token composition.** VL-MoE requests are dominated by image tokens rather than text tokens. As shown in Table 1, visual tokens outnumber text tokens by 3.7× to 18.4× across representative multimodal



(a) Expert-access concentration. (b) Working-set effects of pruning.

**Figure 3.** Spatial impact of token pruning. (a) Pruning redundant visual tokens increases expert-access concentration, improves top- $k$  expert coverage and thus reduces prefill time. (b) This concentration translates into a smaller and more reusable expert working set: the number of inactive experts nearly doubles, on-demand expert loads decrease, and GPU expert hit rate improves during prefill.

benchmarks. Thus, VL-MoE inference is not simply text-centric MoE with a small visual prefix; it operates in a visual-heavy regime, where expert offloading pressure is substantially amplified by the large number of visual tokens.

**Problem 2: Fragmented expert demand.** Token volume alone does not fully explain the difficulty. The more fundamental issue is that raw visual inputs broaden the effective expert working set and reduce routing regularity across layers. As illustrated in Figure 1 and 2, expert accesses under raw visual inputs span a much larger subset of experts than text-centric inputs. This lower locality directly reduces cache residency effectiveness and makes future expert demand harder to predict for lookahead-based offloading.

The next subsection shows that pruning redundant visual tokens helps precisely along these two dimensions: it spatially compacts expert demand within each layer and temporally stabilizes routing behavior across layers, directly addressing both problems above.

### 2.3 Opportunity: Visual-Expert Affinity

Recent visual token compression methods primarily target compute reduction and KV-cache savings [26, 39, 47]. Our profiling reveals an additional systems opportunity for VL-MoE offloading: pruning redundant visual tokens also reshapes expert demand in ways that are directly beneficial for data movement. We refer to this empirical trend as **Visual-Expert Affinity**. Rather than viewing token compression solely as a FLOPs optimization, we observe that it can also improve the locality and predictability properties that efficient expert offloading depends on.

**Spatial concentration.** Token pruning improves the spatial compactness of expert demand within each layer. Many low-information visual patches contribute little to downstream reasoning, yet still inject noisy routing signals and activate a broad set of experts. As shown in Figure 3(a),

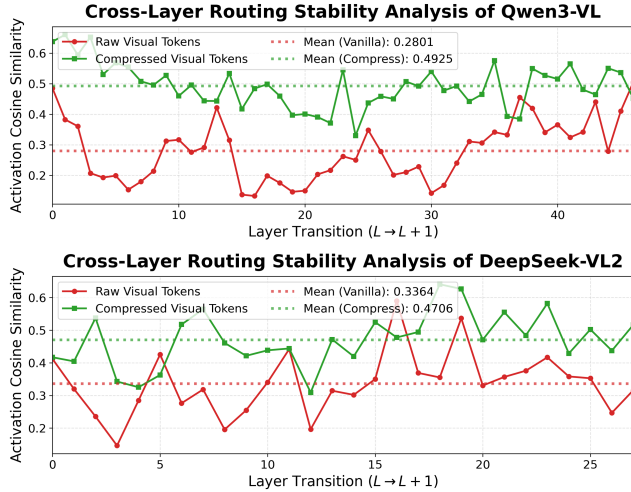


**Figure 4.** Temporal impact of token pruning. Pruning redundant visual tokens increases inter-layer routing similarity, making future expert demand more predictable for lookahead-based prefetching.

pruning such redundant tokens increases top- $k$  expert coverage and concentrates routing onto a smaller expert subset. This concentration shrinks the effective on-demand expert set: Figure 3(b) shows that more experts remain inactive, on-demand expert loads decrease, and GPU expert hit rate improves during prefill. Thus, even without prediction or prefetching, spatial concentration alone already lowers prefill offloading overhead.

**Temporal stability.** Token pruning also improves routing regularity across layers. Owing to the residual structure of Transformer backbones, hidden states—and thus MoE gating inputs—are naturally similar across nearby layers. Raw visual tokens, however, inject noisy and fragmented routing signals that weaken this cross-layer consistency and make future expert demand harder to anticipate. As shown in Figure 4, raw visual tokens exhibit lower inter-layer routing similarity than text-centric inputs. After pruning, the retained tokens induce more stable gating trajectories across consecutive layers. This increased temporal stability makes the expert working set of subsequent layers more predictable, thereby improving the effectiveness of lookahead-based prefetching.

Together, these observations show that visual token compression can serve not only as a compute reduction, but also as a systems optimizer in offloading. It motivates a design that aligns token retention with expert locality and future expert demand, which we present in the next section.

### 3 VisMMOE System

#### 3.1 VisMMOE Overview

The challenges and opportunities discussed in Section 2 highlight the need for a VL-MoE offloading design that goes

beyond simplistic per-layer prefetching. To this end, we present *VisMMOE*, an offloading system that explicitly leverages Visual-Expert Affinity. By compacting expert demand, enabling deeper lookahead prediction, and coordinating data movement, *VisMMOE* reduces exposed PCIe transfer overhead and improves end-to-end inference efficiency under tight memory budgets. Figure 5 illustrates the architecture of *VisMMOE*, which consists of three components for efficient VL-MoE offloading:

- **Affinity-aware Token Compressor.** This module retains visual tokens according to semantic importance and expert affinity. It reduces the effective expert working set and makes expert activations more concentrated, improving both transfer efficiency and cross-layer predictability.
- **Compression-Guided Lookahead Predictor.** Using the condensed visual signals from the compression module, this module estimates the experts required in future layers, enabling lookahead for prefetching.
- **Expert Caching and Pipeline Orchestrator.** Based on the predicted expert working sets, this module coordinates GPU memory, including a small resident prefix for routing observability, PCIe transfers, and model execution so that expert movement can be largely overlapped with computation whenever possible.

The three components of *VisMMOE* are tightly coupled. Affinity-aware compression reshapes expert demand, enabling more accurate prediction and more effective cache/pipeline orchestration. Without this demand-shaping effect, both prediction and cache reuse degrade under visual-heavy inputs.

#### 3.2 Affinity-aware Token Compressor

To operationalize *Visual-Expert Affinity*, we design **Affinity-aware Token Compressor**, a visual-token selection policy tailored for VL-MoE offloading as shown in Algorithm 1. Unlike prior compression methods that primarily optimize FLOPs or KV-cache usage, our objective is explicitly system-facing: under a fixed keep budget, retain tokens that preserve useful visual evidence while limiting unnecessary expansion of the expert working set. Intuitively, once the indispensable visual evidence has been preserved, the remaining token budget should not simply be spent on the next-most-salient tokens in isolation; it should be spent on tokens that add useful context with minimal additional expert demand. Formally, let  $V = \{v_i\}_{i=1}^N$  denote the visual tokens, and let  $K_{\text{keep}} = \lfloor \beta N \rfloor$  be the total keep budget under keep ratio  $\beta$ . Our design proceeds in two steps. We first identify a salient core that serves as an accuracy anchor, and then allocate the remaining budget using a calibrated working-set-aware score.

**3.2.1 Salient Core as an Accuracy Anchor.** We first identify a small set of visually indispensable tokens that anchors semantic fidelity. Importantly, this *salient core* is

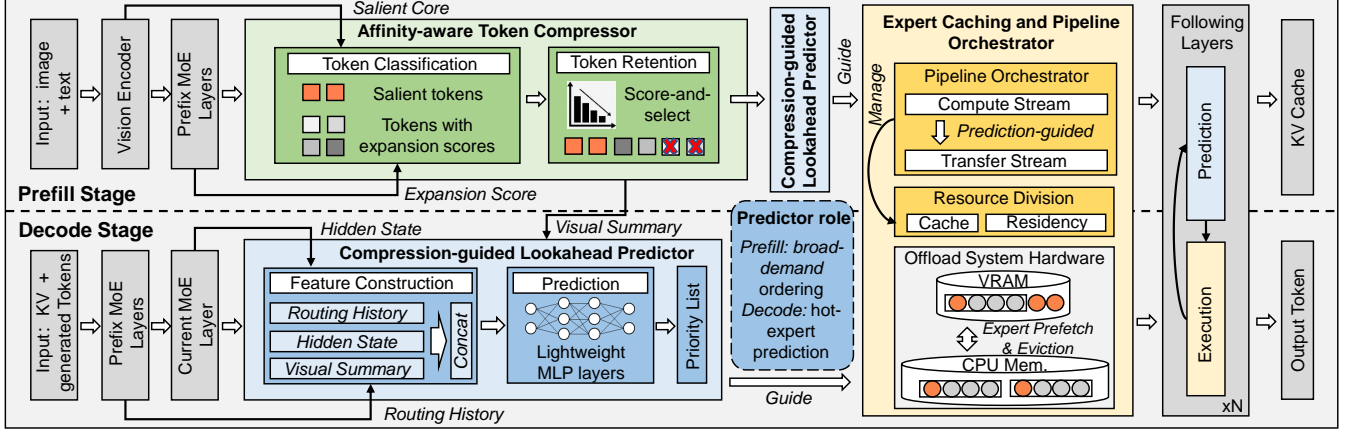


**Figure 5.** Overview of the *VisMMOE* architecture. In prefill, raw multimodal inputs are compressed by the *Affinity-aware Token Compressor*. The *Compression-guided Lookahead Predictor* produces phase-dependent priority signals: broad-demand ordering in prefill and hot-expert prediction in decode. Guided by these signals, the *Expert Caching and Pipeline Orchestrator* manages cache residency and overlaps expert transfer with execution.

### Algorithm 1: Affinity-Aware Token Compression

**Input** : Attention maps  $A$ , prefix routing outputs  $R$ , salient ratio  $\alpha$ , keep ratio  $\beta$ , trade-off weight  $\lambda$   
**Output** : Retained token indices  $I_{\text{keep}}$

- 1  $N \leftarrow |A|$
- 2  $s \leftarrow \text{Mean}_h(A^h)$  // Head-averaged token saliency
- 3  $\tilde{s} \leftarrow \text{Normalize}(s)$  // Normalize to  $[0, 1]$
- 4  $K_{\text{core}} \leftarrow \lfloor \alpha N \rfloor$ ,  $K_{\text{keep}} \leftarrow \lfloor \beta N \rfloor$ ,  $K_{\text{rem}} \leftarrow K_{\text{keep}} - K_{\text{core}}$
- 5  $I_{\text{core}} \leftarrow \text{TopK}(\tilde{s}, K_{\text{core}})$  // Salient core
- 6  $\mathcal{E}_{\text{target}} \leftarrow \bigcup_{j \in I_{\text{core}}} \text{ActiveExperts}(R_j)$  // Core-induced expert set
- 7 **foreach**  $i \notin I_{\text{core}}$  **do**
- 8      $\mathcal{E}_i \leftarrow \text{ActiveExperts}(R_i)$
- 9      $\Delta_i \leftarrow |\mathcal{E}_i \setminus \mathcal{E}_{\text{target}}| / |\mathcal{E}_i|$  // Marginal expansion
- 10     $p_i \leftarrow \tilde{s}_i - \lambda \Delta_i$  // Working-set-aware score
- 11 **end**
- 12  $I_{\text{extra}} \leftarrow \text{TopK}(p, K_{\text{rem}})$ ,  $I_{\text{keep}} \leftarrow I_{\text{core}} \cup I_{\text{extra}}$
- 13 **return**  $I_{\text{keep}}$

not the final compressed set; rather, it provides an accuracy-preserving foundation on top of which the remaining keep budget is allocated. Keeping only the most salient tokens is often too aggressive for downstream VL reasoning, while retaining additional context remains beneficial as long as it does not excessively expand expert demand.

Following standard visual token compression practice [26, 47], we estimate token saliency from the attention maps of the vision encoder. Let  $A$  denote the attention tensor and let  $s_i$  be the head-averaged saliency score of token  $v_i$ . We then normalize saliency scores to  $\tilde{s}_i \in [0, 1]$  and retain the top  $K_{\text{core}} = \lfloor \alpha N \rfloor$  tokens as the salient core:

$$I_{\text{core}} = \text{TopK}(\tilde{s}, K_{\text{core}}), \quad (1)$$

where  $\alpha$  is a small salient ratio. These tokens preserve the most important visual evidence and define the minimum semantic context that should not be discarded.

The salient core also induces an *unavoidable* expert set. Specifically, we use router outputs from the pinned prefix of early MoE layers and, for each token, collect the experts it activates across those layers; their union defines the token’s active expert set for affinity scoring. The expert set induced by the core tokens therefore captures the prefix-scoped expert working set already required to preserve the visual semantics. The remaining compression problem is thus not simply which tokens are salient in isolation, but which additional tokens provide useful context with minimal expansion cost. This prefix-scoped expert representation is used only for compression-time affinity scoring and is distinct from the predictor output space in Section 3.3.

**3.2.2 Calibrated Marginal Expansion Score.** Given the salient core, we allocate the remaining token budget using a **calibrated marginal expansion score**. The goal is to retain additional tokens that preserve useful visual context while introducing as little new expert demand as possible beyond the core-induced expert set.

For each non-core token  $v_i$ , let  $E_i = \text{ActiveExperts}(R_i)$  denote the experts activated by that token. We define its marginal expansion score relative to the salient core as

$$\Delta_i = \frac{|E_i \setminus E_{\text{target}}|}{|E_i|}. \quad (2)$$

Equivalently, if  $m_i \in \{0, 1\}^E$  and  $m_{\text{target}} \in \{0, 1\}^E$  denote the corresponding multi-hot expert masks, then

$$\Delta_i = \frac{\|m_i \odot (1 - m_{\text{target}})\|_1}{\|m_i\|_1}. \quad (3)$$

This score measures how much new expert demand a token would introduce beyond the current core-induced working set. Tokens that largely reuse the core-induced experts incur low marginal expansion, while tokens that introduce many new experts incur high marginal expansion.

Based on this score, we rank non-core tokens by

$$p_i = \tilde{s}_i - \lambda \Delta_i \quad (4)$$

where  $\lambda$  balances semantic value against working-set growth. We use a fixed global value of  $\lambda = 2$  throughout the evaluation since ?? shows that this setting captures most of the latency benefit while preserving competitive accuracy. Since both  $\tilde{s}_i$  and  $\Delta_i$  are normalized to  $[0, 1]$ , this value assigns twice the weight to working-set expansion as to semantic saliency, reflecting the I/O-dominated nature of expert off-loading. This single value is shared across all models and benchmarks. The final retained set is

$$I_{\text{keep}} = I_{\text{core}} \cup \text{TopK}(\{p_i\}_{i \notin I_{\text{core}}}, K_{\text{keep}} - K_{\text{core}}). \quad (5)$$

This score-guided allocation explains why we do not stop at the top- $\alpha N$  salient tokens. The salient core anchors accuracy, while the remaining budget preserves additional context in a working-set-aware manner, yielding a compressed set that retains more useful visual evidence than core-only pruning and induces a smaller, more reusable expert working set than saliency-only retention. Since affinity-aware selection requires routing signals unavailable from raw visual inputs, we derive them from a small pinned prefix of early MoE layers on GPU, whose router outputs expose the expert structure needed for scoring; its broader runtime role is discussed in Section 3.4.

### 3.3 Compression-guided Lookahead Predictor

We introduce a **compression-guided lookahead predictor** that runs alongside the main execution loop (Figure 6) and provides an early priority signal for near-future expert demand. In **prefill**, where demand is broader, this signal serves mainly as a bounded priority ordering under limited VRAM and bandwidth: higher-scored experts are fetched earlier, improving overlap and cache residency, while experts absent from the realized routes need not be fetched. In **decode**, where demand is much sparser and more reusable, the same signal more directly identifies near-future hot experts and avoids unnecessary prefetches.

**3.3.1 Compression-aware Feature Construction.** At MoE layer  $l$ , the predictor forms a compact feature vector  $\mathbf{x}_l$  from three signals: (i) **routing history**  $\mathbf{h}_l^{(r)} \in \mathbb{R}^{D_r}$ , a compressed histogram of recent expert activations; (ii) **compressed hidden-state summary**  $\mathbf{h}_l^{(h)} \in \mathbb{R}^{D_h}$ , obtained by pooling only over the retained visual tokens from Section 3.2; and (iii) **compressed visual summary**  $\mathbf{h}^{(v)} \in \mathbb{R}^{D_v}$ , a static visual descriptor computed from the same retained token

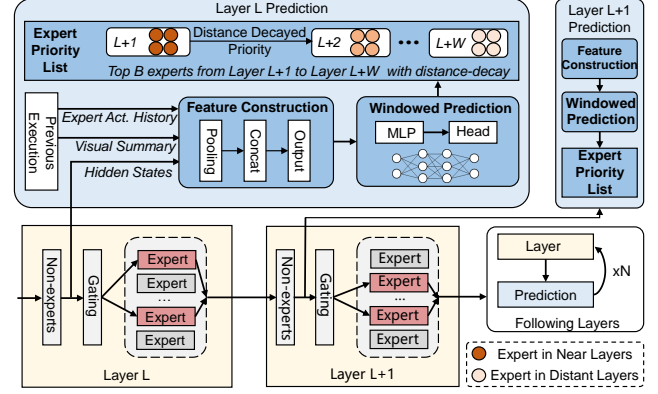


**Figure 6.** Architecture of the compression-guided lookahead predictor. The predictor pools compressed hidden-state and visual summaries from the retained token set, combines them with routing history, and predicts a priority score over experts within a bounded lookahead window.

set. Let  $\bar{I}_{\text{keep}}$  denote the retained visual-token indices after affinity-aware compression. We define:

$$\mathbf{h}_l^{(h)} = \text{MP}(\{\mathbf{h}_{l,j} : j \in \bar{I}_{\text{keep}}\}), \quad \mathbf{h}^{(v)} = \text{MP}(\{\mathbf{v}_j : j \in \bar{I}_{\text{keep}}\}). \quad (6)$$

where  $\mathbf{h}_{l,j}$  is the hidden state of retained token  $j$  at layer  $l$ , and  $\mathbf{v}_j$  is its corresponding visual embedding. By mean pooling (MP) only over the affinity-aware compressed tokens, the predictor both reduces its feature-processing cost and suppresses noisy visual patches. The final predictor input is

$$\mathbf{x}_l = [\mathbf{h}_l^{(r)}; \mathbf{h}_l^{(h)}; \mathbf{h}^{(v)}]. \quad (7)$$

During autoregressive decoding, repeatedly reading the retained visual hidden states from the KV-cache would incur prohibitive memory bandwidth. Therefore, we reuse the static visual summary  $\mathbf{h}^{(v)}$  throughout decode.

**3.3.2 Windowed Prediction with Decayed Supervision.** Rather than predicting expert usage across all remaining layers, we predict a bounded *lookahead window* of the next  $W$  layers. This is the horizon most relevant to prefetching under limited VRAM, since experts needed much later should not compete with imminent experts for bandwidth and cache residency. The predictor is implemented as a lightweight bottleneck MLP:

$$\mathbf{z}_l = \psi(\mathbf{W}_2 \psi(\mathbf{W}_1 \mathbf{x}_l)), \quad \mathbf{y}_l = \mathbf{W}_o \mathbf{z}_l, \quad (8)$$

where  $\psi$  denotes the BN-ReLU-Dropout block, and  $\mathbf{y}_l \in \mathbb{R}^E$  gives an expert-priority score over the global expert pool.

To bias the predictor toward nearer layers within the lookahead window, we use a decayed supervision target. Let  $\mathcal{E}_{l+d}$  denote the experts activated at layer  $l+d$ . For expert  $e$ , the target score is

$$g_{l,e} = \max_{1 \leq d \leq W} \gamma^{d-1} \mathbb{I}[e \in \mathcal{E}_{l+d}], \quad (9)$$

where  $\gamma \in (0, 1]$  is a distance-decay factor. Near-future experts therefore receive higher priority than experts that

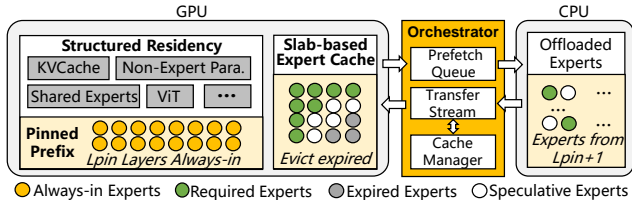


Figure 7. Data layout of *VisMMOE*.

appear in deeper layers of the lookahead window. At runtime, the scheduler uses the top- $B$  entries of  $\mathbf{y}_l$  as an ordered prefetch candidate set: in prefill, it is a bounded priority list rather than an exact cover of future experts, whereas in decode it more directly tracks near-future hot experts.

**3.3.3 Per-layer Rolling Prediction and Runtime Integration.** The prediction module is invoked once at every MoE layer, continuously refreshing expert priorities as routing context evolves across depth. In **prefill**, rolling updates refine the ordering of a relatively broad future working set; in **decode**, they track a much sparser and more reusable set of near-future experts. At layer  $l$ , the module outputs an expert-priority vector  $\mathbf{y}_l$ , from which the runtime extracts the top- $B$  candidates for prefetch. The module requires only lightweight one-time calibration for a target VL-MoE family and is trained with soft binary cross-entropy on the distance-decayed targets  $\mathbf{g}_l$ . Unless otherwise stated, we use  $W=5$ ,  $\gamma=0.8$ ,  $B=20$ , and mean pooling for both compressed hidden-state and visual summaries. Because prediction operates on compact summary features rather than full token states, its overhead is small in practice and can be largely overlapped with ongoing execution; quantitative breakdown is reported in Section 4, and implementation details are provided in ??.

### 3.4 Expert Caching and Pipeline Orchestrator

To support asynchronous deep prefetching under limited VRAM, we divide GPU memory into a *static resident region* and a *dynamic slab-based expert cache*, as shown in Figure 7. The resident region keeps latency-critical parameters permanently on GPU, while the dynamic cache manages deeper experts online. Guided by the predictor, the **Expert Caching and Pipeline Orchestrator** uses near-future expert priorities to drive both prefetching and replacement.

**3.4.1 Structured Residency for Latency Masking.** The static resident region both preserves non-swappable parameters and creates an initial overlap window in which deeper-layer transfers can proceed concurrently with computation. **Always-resident components.** Shared experts, which show near-100% hit rates, remain permanently pinned. Non-expert backbone parameters (e.g., attention blocks) are likewise kept resident by the base runtime.

### Pinned prefix for routing context and startup overlap.

We keep the *entire expert pool* of the first  $L_{\text{pinned}}$  MoE layers resident on GPU. This pinned prefix serves two roles: it exposes the early routing signals required by affinity-aware compression and lookahead prediction, and it creates a startup overlap window for asynchronously prefetching deeper experts before steady-state offloading begins. Since compression takes effect only after the pinned prefix, these layers run on the uncompressed token stream. Because all experts in the prefix are resident, this stage incurs no PCIe I/O overhead, and its extra FLOPs are largely hidden by overlap with deeper-layer prefetching. Under a fixed VRAM budget, *VisMMOE* chooses a compact prefix that is sufficient for routing observability and startup overlap, leaving the remaining memory for the dynamic cache.

The prefix depth  $L_{\text{pinned}}$  is chosen at deployment time. Let  $M_{\text{avail}}$  denote the expert VRAM budget and  $S_{\text{layer}}$  the footprint of one full MoE layer. We define the valid prefix interval as

$$\mathcal{I}_{\text{valid}} = \left\{ L \in \mathbb{N} \mid L_{\text{semantic}} \leq L \leq \left\lfloor \frac{M_{\text{avail}} - C_{\text{safe}}}{S_{\text{layer}}} \right\rfloor \right\}, \quad (10)$$

where  $L_{\text{semantic}}$  is the minimum depth at which routing context becomes sufficiently informative.  $C_{\text{safe}}$  is the minimum memory reserved for the dynamic cache. ?? provides the corresponding empirical evidence.

**3.4.2 Dynamic Slab-Based Expert Cache.** The remaining VRAM is organized as a dynamic cache for deep MoE layers ( $L > L_{\text{pinned}}$ ). To avoid fragmentation and runtime allocation overhead (e.g., `cudaMalloc`), we pre-partition this space into fixed-size slabs, each storing one expert.

**Lookahead-driven insertion.** At each MoE layer, the predictor produces a priority vector  $\mathbf{y}_l$  on GPU, which is asynchronously copied to the host. The host-side transfer stream  $S_{\text{trans}}$  continuously polls this state and issues back-to-back DMA transfers for the highest-priority pending experts, avoiding synchronization stalls on the critical path.

**Safety-guarded eviction.** When a cache slab must be reclaimed during autoregressive decoding, an expert is eligible for eviction only after its layer has completed execution for the current token. As shown in Figure 7, dynamically cached experts are divided into **Required Experts**, protected within the current lookahead window; **Speculative Experts**, temporarily retained to absorb short-term prediction shifts; and **Expired Experts**, which have completed execution and are no longer protected. When space is needed, the cache manager evicts only **Expired Experts**, prioritizing those with the lowest predictor-derived priority. This policy ensures eviction safety while preserving limited prediction-guided reuse across decoding steps.

**3.4.3 I/O-Aware Pipeline Orchestration.** In deep MoE offloading, PCIe transfer time typically dominates computation ( $T_{\text{trans}} \gg T_{\text{comp}}$ ). Lookahead prediction therefore does

**Table 2.** Configuration of two evaluated MMoE models.

	Qwen3-VL-30B-A3B	Deepseek-VL2
Total Parameters	30B	27B
Activated Parameters/Token	3.3B	4.5B
Per expert size	17.3 MB	23.6 MB
Total Weight Size	62GB	55GB
Layer Number	48	30
Expert Number/Layer	128	72
Activated Expert/Token	8	6+2(shared)

not remove transfer demand, but shifts it off the critical path by turning reactive fetches into background prefetches.

We decouple execution into a transfer stream ( $S_{\text{trans}}$ ) and a compute stream ( $S_{\text{comp}}$ ). At each MoE layer, the predictor refreshes expert priorities and  $S_{\text{trans}}$  fetches the highest-priority pending experts, while  $S_{\text{comp}}$  executes resident layers together with the lightweight predictor. Affinity-aware compression reduces the effective expert working set, and the predictor concentrates bandwidth on near-future demand, allowing the transfer stream to stay ahead of computation.

If a required expert is not yet resident,  $S_{\text{comp}}$  stalls only on that expert, while  $S_{\text{trans}}$  continues draining the remaining queue. As a result, imperfect prediction causes localized misses rather than pipeline-wide stalls.

## 4 Evaluation

### 4.1 Experimental Setup

**4.1.1 Hardware.** To evaluate VisMMOE under different memory-constrained deployment settings, we conduct experiments on three representative platforms. First, to study a server-class setting where strong compute capability is still limited by GPU memory capacity, we use a workstation with a single NVIDIA A100 GPU equipped with 40 GB HBM [30]. We also evaluate on a single NVIDIA RTX 3090 GPU with 24 GB memory, representing a more constrained commodity high-end GPU setting. In both cases, the GPUs are attached to sufficient host memory, enabling GPU/CPU offloading without host-memory bottlenecks.

Second, to explore a more constrained embedded setting, we use an NVIDIA Jetson AGX Orin [31] with 32 GB shared memory. For model-weight storage, we use a Samsung 980 PRO SSD [33], which provides a theoretical sequential read bandwidth of 7,000 MB/s and around 3,000 MB/s in our practical setup. As discussed later, the Orin experiments rely on an OS-managed memory hierarchy via Linux swap, rather than a dedicated framework-level SSD offloading path or a custom direct NVMe-to-GPU paging implementation.

**4.1.2 Implementation.** We implement VisMMOE on top of two representative serving frameworks, Hugging Face Accelerate [12] and KTransformers [4], by modifying their memory management and execution flow with approximately 6,000 lines of Python and C++ code. Unlike conventional

coarse-grained layer-wise offloading, VisMMOE partitions available memory into a *Static Resident Region* and a *Dynamic Expert Cache*, enabling different execution modes under different hardware constraints.

**Offload-only Mode.** In this mode, offloaded experts are fetched from host memory to GPU memory on demand. The main execution thread invokes the Deep Lookahead Predictor to estimate future hot experts, while the Pipeline Orchestrator asynchronously prefetches missing experts through host-to-device transfers. Computation on already resident experts proceeds in parallel with these transfers, so host memory serves as a high-capacity backing store and the runtime focuses on maximizing compute-I/O overlap.

**GPU-CPU Hybrid Mode.** In this implementation, when the scheduler detects that a miss would stall the pipeline, it can dispatch the corresponding token activations to the CPU instead of transferring the expert weights. A worker thread executes the expert directly in host memory using optimized AVX/AMX kernels, and synchronizes the results back to the GPU. This design reduces bursty host-to-device traffic and provides a bounded fallback path under cache misses or prediction errors.

**Platform-specific deployment.** On server-class GPUs, we use GPU/CPU offloading through the host-memory-based execution path supported by the underlying frameworks. On Jetson Orin, because no mature framework-level SSD offloading path is available for the evaluated VL-MoE models, we rely on Linux swap to extend effective host memory capacity onto SSD. Accordingly, the Orin results reflect an OS-managed memory hierarchy rather than a custom direct NVMe-to-GPU paging design.

**4.1.3 Models.** We select two representative mainstream MoE models in Table 2 that exhibit substantial differences in overall scale, architectural design, and MoE layer implementation. This diverse selection enables a more comprehensive and rigorous evaluation of our system’s scalability and generalization capability across heterogeneous configurations.

**4.1.4 Datasets.** To rigorously evaluate VisMMOE across diverse modalities and difficulty levels, we select four representative benchmarks: MME [10] and MMBench-EN [27] for comprehensive multi-modal perception and reasoning; POPE [23] for evaluating object hallucination and fine-grained visual consistency; OCRBench [28] for OCR capabilities.

**4.1.5 Baselines.** We evaluate our system against three representative baselines. The first is the hugging face accelerate [12] (AC), a general LLM library providing basic support for transformers. The second is the slang [52] (SG), a high-performance serving framework for large language models. The third is the ktransformer [4] (KT), a CPU-optimized framework for heterogeneous LLM inference which specifically optimizes MOE offloading. We built VisMMOE both on

**Table 3.** Performance comparison with Vanilla (100%) baseline and different pruning ratios (70%, 50%). *VisMMOE* reaches comparable accuracy with Vanilla and SOTA visual token compression methods [47].

Dataset	Qwen3-VL-30B-A3B					DeepSeek-VL2													
	Vanilla	Random		Zip		Mix	VisMMOE	Vanilla	Random		Mix	VisMMOE							
	100%	70%	50%	70%	50%	70%	50%	100%	70%	50%	70%	50%							
MME	2498	2181	2053	2475	2309	2375	2212	2470	2299	MME	2243	2115	2014	2195	2142	2153	2090	2178	2103
OCRBench	829	674	554	819	741	793	685	801	705	OCRBench	803	631	591	780	685	761	646	771	673
POPE	90.02	89.8	88.3	90.1	89.6	90.01	89.6	90.1	89.6	POPE	88.42	87.4	85.2	88.1	87.3	87.7	86.9	88.2	87.3
MMBench	86.4	82.6	80.15	84.8	83.7	83.3	82.9	84.6	83.5	MMBench	77.4	75.1	72.5	76.6	75	76.0	74.1	76.5	74.7

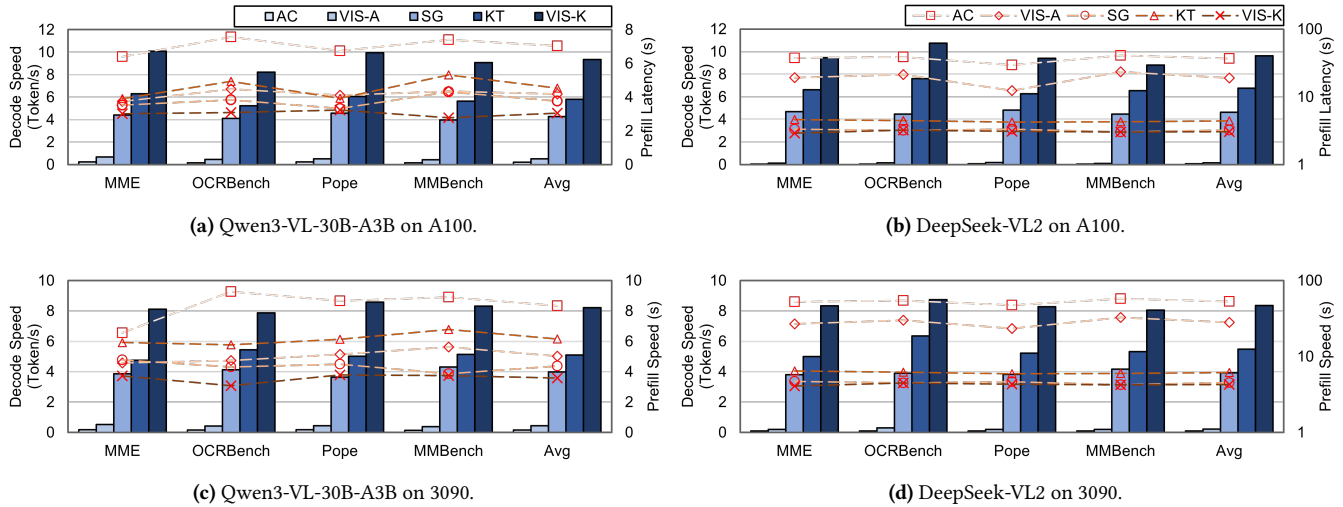


**Figure 8.** Comparison of End-to-End inference speed for *VisMMOE* and the SOTA approaches. *VisMMOE* achieves best performance on all tasks and hardware platforms in both prefill and decode stages.

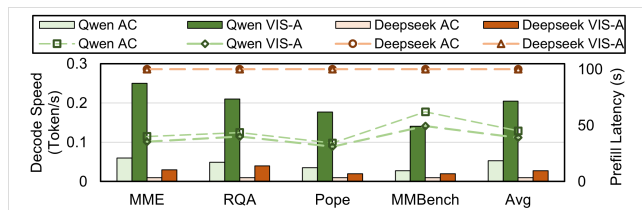


**Figure 9.** *VisMMOE* inference speed on Orin. Currently, ssglang and ktransformers fails to support SSD swap on Orin.

accelerate and ktransformer, creating two versions of *VisMMOE* (VIS-A and VIS-K). All experiments are conducted under 50% pruning ratio.

Currently, prior academic MoE offloading systems such as MoE-Infinity [46], MoE-Offloading [7], and HOBbit [40] are primarily designed for text-centric MoE workloads and do not provide support for the VL-MoE models evaluated in this paper. As a result, we do not include them in our experimental comparison. We therefore limit our empirical claims to the baselines that can be run reliably on the target VL-MoE models and hardware platforms.

## 4.2 Comparison with SOTA

### 4.2.1 Model Accuracy.

Since we prune less important tokens, it is crucial to verify that *VisMMOE* does not sacrifice performance. Table 3 reports the performance comparison between *VisMMOE* and various baselines, including full-loading and other pruning strategies, across different compression ratios. *VisMMOE* achieves accuracy comparable to state-of-the-art token compression methods (e.g., VisionZip) while significantly reducing the token count. Compared with the Vanilla (100%) accuracy baseline, *VisMMOE* (70%) only shows 1.12%, 3.38%, -0.09% (gain) and 2.08% of accuracy downgrade respectively for *MME*, *OCRBench*, *POPE* and *MMBench* on Qwen3-VL, suggesting that our affinity-aware pruning may effectively filter out visual routing noise. The only noticeable performance gap occurs in *OCRBench* when we prune 50% of the visual tokens, which is highly sensitive to high-resolution visual details. While a slight drop is observed, *VisMMOE* still significantly outperforms random pruning and remains competitive with SOTA token compression methods. This confirms that *VisMMOE* effectively balances system efficiency with reasoning fidelity.

**Table 4.** Ablation: speed and memory budget breakdown.

Qwen3-VL-30B-A3B			
Implementation	Method	Speed (s)	Norm.
Hugging Face Transformers	Base (pure transformer)	13.17	100%
	+ compression	11.55 (-1.62)	87.7%
	+ prediction & prefetching	7.72 (-5.45)	58.6%
	+ optimization (VisMMOE)	4.91 (-8.26)	37.2%
KTransformers	Base (pure KTransformers)	3.89	100%
	+ compression	3.71 (-0.18)	95.3%
	+ prediction & prefetching	2.34 (-1.55)	60.1%
	+ optimization (VisMMOE)	2.21 (-1.68)	56.8%
A100-40GB memory	anchor: 21.6 GB	static: 4.1 GB	cache: 14.3 GB

**4.2.2 End-to-end Performance.** From Figure 8a and Figure 8b, we can observe that *VisMMOE* delivers the best performance in terms of both decoding speed and prefill latency for the evaluated models. The *VisMMOE* implementation based on Accelerate [12] performs 2.68x and 2.29x better in decode speed, and possess 52% and 58.7% of prefill latency respectively for Qwen and Deepseek-VL2. Note that the huggingface implementation of Deepseek-VL2 offload is extremely inefficient as it is based on old frameworks (torch 2.0.1) with customized implementation. For ktransformer-based [4] *VisMMOE* implementation, Vis-K also performs 1.61x and 1.42x better in decode speed. VIS-K achieves 34% and 31% of prefill latency reduction. Ktransformer performs poor in prefill stage since it has to compute large proportion of experts on CPU (all experts are involved in prefilling while only 6-8 in decode). In contrast, *VisMMOE* tries to compute hot experts on GPU. Vis-K also significantly outperforms sglang [52], which is a widely used serving framework.

Similar conclusions can be drawn on RTX 3090 as shown in Figure 8c and 8d. The *VisMMOE* implementation on accelerate achieves up to 2.53x decode speedup and 47% of prefill reduction compared with accelerate, while the *VisMMOE* implementation on ktransformer achieves up to 1.54x decode speedup and 37% of prefill reduction.

Additionally, we experiment on Jetson Orin as shown in Figure 9. Unfortunately, sglang [52] and ktransformers [4] fail to support SSD swap on Orin with 32GB unified memory. They suffer severe *NvMapMemAllocInternalTagged* error in load weight stage. While VIS-A actually outperforms accelerate [12] more on Jetson due to the low SSD bandwidth in swapping, the extremely low decode speed and high prefill latency prevents it from practical usage.

### 4.3 Ablation Study

**4.3.1 Speedup Breakdown.** The ablation study in Table 4 demonstrates the individual and combined impact of three key optimizations in *VisMMOE*: affinity-aware compression, prediction-guided prefetching, and pipeline optimization. When all optimizations are enabled, the system achieves a latency of 4.91s (37.2% normalized) on the Huggingface

backend. Disabling the deep prediction and pipeline optimization (i.e., using only compression) increases latency to 11.55s (87.7%), indicating a modest but measurable benefit derived solely from I/O volume reduction. In contrast, enabling prediction and prefetching leads to a more significant drop to 7.72s (58.6%), highlighting its substantial contribution to performance by effectively masking the massive expert transfer overhead. When all optimizations are removed, performance further degrades to 13.17s. Notably, the performance gains from stacking these components are cumulative, suggesting that compression acts as an enabler for the predictor, while the pipeline orchestrator ensures the theoretical bandwidth gains are realized in practice.

*VisMMOE* also achieves 1.76x speedup on ktransformers. Compression show limited effects as ktransformer is already well-optimized and I/O far overweigh computation. Most of the benefits comes from predicting and placing hot experts on GPU both in prefill and decode stages.

For Qwen3-VL-30B-A3B on A100-40GB, VRAM is divided among the backbone, pinned anchor layers, and the dynamic expert cache. The backbone occupies 4.1 GB, anchor layers take 21.6 GB, and the remaining 14.3 GB is used for the cache. This illustrates the tradeoff in *VisMMOE*: deeper anchoring improves early routing visibility for prediction, but reduces cache capacity for later-layer experts. On RTX 3090, the tighter VRAM budget allows us to pin only the first four layers, which weakens prediction and shortens the effective prefetch window. As reflected in our main results, this leads to smaller end-to-end gains on the 3090 than on the A100.

**4.3.2 Prediction Accuracy.** We evaluate the effectiveness of our Predictor using Hot Recall, the ratio of activated experts successfully prefetched into the cache. As illustrated in Figure 10, the predictor significantly outperforms the random baseline, which yields a meager recall of 7.8% ( $k = 10$ ) to 23.4% ( $k = 30$ ). In stark contrast, *VisMMOE* achieves 64.1%, 81.9%, and 89.8% for buffer sizes of  $k = 10, 20, 30$  respectively on five different datasets. This represents a massive  $3.8\times$  to  $8.2\times$  improvement, confirming that our affinity-aware visual compression successfully exposes predictable routing patterns. While the predictor is trained on partial data of *MME*, *OCRBench*, *MMBench* and *Pope*, it also shows similar effect on *textvqa* which does not participate in training at all. It proves the versatility of our predictor.

**4.3.3 Effect of visual information on expert prediction.** Figure 11 highlights the importance of visual information in expert prediction. We compare the full predictor with an already competitive ablated variant that relies only on hidden states and historical routing traces, without the ViT visual feature ( $h_l^{(v)}$ ). This ablated predictor is substantially stronger than a random or history-free baseline, since it still captures evolving textual states and prior expert activation

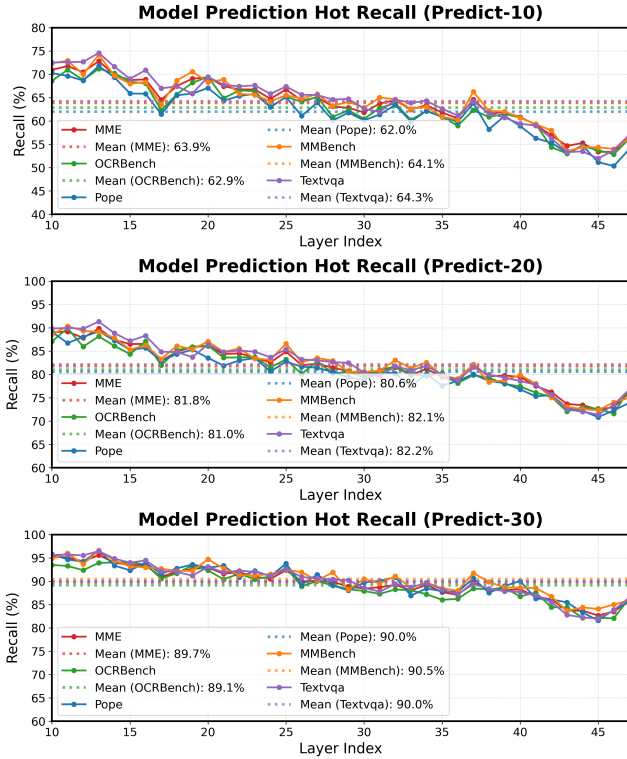


**Figure 10.** Layer-wise *Hot Recall* performance of the expert predictor on different datasets. The proposed predictor significantly outperforms the random baselines by 3.82x (predict-30) to 7.9x (predict-10). Note that the *VisMMOE* predictor works well even for *textvqa*, which does not participate in training at all. Layers 0-9 are pinned on the GPU memory and do not require prediction.

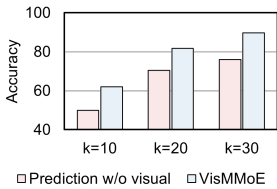


**Figure 11.** The effect of visual info in prediction.

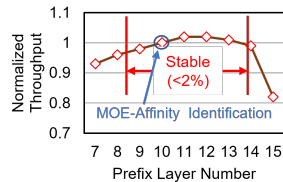


**Figure 12.** Anchor layer number choice and effect.

patterns. Nevertheless, its Hot Recall drops markedly across all prediction horizons once visual features are removed.

**4.3.4 Anchor layer number choice and effect.** Figure 12 plots the end-to-end execution time across different  $L_{\text{pinned}}$  values. The results reveal a clear U-shaped performance curve with a distinct, stable optimal region (e.g.,  $L_{\text{pinned}} \in [8, 12]$  for Qwen3-VL). *VisMMOE*'s offline profiling successfully identifies and selects an anchor size within this region.

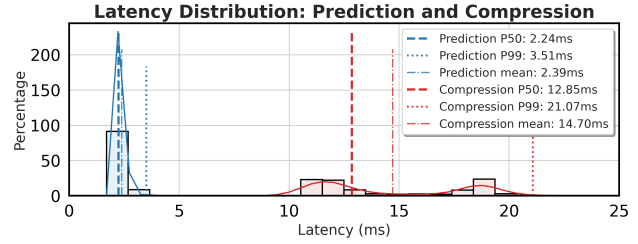


**Figure 13.** *VisMMOE* compression and predictor costs. Presented in latency distribution.

This empirical analysis confirms that *VisMMOE*'s offline selection effectively balances prediction accuracy, initial latency masking, and steady-state cache stability.

**4.3.5 Prediction/Compression Cost.** To assess the runtime cost of our introduced modules, we profile the latency distribution of the Affinity-Aware Token Compression and the Compression-Guided Predictor, as illustrated in Figure 13. The predictor proves to be extremely lightweight, introducing a negligible overhead with a mean latency of 2.72 ms (P50: 2.78 ms, P99: 3.15 ms). This sub-3ms latency is orders of magnitude smaller than the expert transfer time (tens of ms), ensuring that the lookahead mechanism essentially runs for free alongside the main computation. The compression module incurs a moderate one-time cost, averaging 14.70 ms (P50: 12.85 ms, P99: 21.07 ms). While higher than prediction, this overhead is strategically masked. As detailed in Section 3.4, compression is performed only once during the execution of the resident layers.

## 5 Related Works

**Visual Token Compression:** Visual token compression has become an important optimization under high-resolution images and long visual sequences [32]. Existing methods [5, 15, 22, 54], such as VisionZip [47], mainly remove *intra-image redundancy* by selecting salient or non-redundant patches using saliency signals, similarity metrics, or learned policies [1, 26, 35, 39, 47, 49]. FastMMOE [43] first take routing into consideration in token compression. However, these methods mainly optimize algorithmic efficiency, such as reducing FLOPs or KV-cache growth, without explicitly considering downstream expert offloading behavior. *In contrast, VisMMOE uses visual token compression as a systems lever to compact the expert working set and improve expert predictability during offloaded VL-MoE inference.*

**General LLM Inference Systems:** A large body of work improves LLM serving efficiency through better memory management, batching, and operator optimization. Systems such as vLLM [19] and DeepSpeed [2] improve throughput and latency through optimized runtime support, while Accelerate [12] and llama.cpp [11] enable deployment on memory-constrained devices via CPU or NVMe offloading.

Other systems, including DeJa Vu [29], PowerInfer [38], and CATS [20], exploit activation sparsity in dense models to skip redundant computation. However, these systems mainly target dense models or general-purpose serving, rather than the dynamic expert movement bottleneck in sparse MoE inference. *In contrast, VisMMOE targets offloaded VL-MoE inference and optimizes expert locality, prefetchability, and cache efficiency under limited GPU memory.*

**Expert Offloading for MoE-based Models:** Prior work reduces the memory footprint of MoE models by streaming experts on demand. Systems such as MoE-Offloading [7], MoE-Infinity [46], and SwapMoE [18] hide I/O latency through expert prefetching and cache management, while KTransformers [4] and Fiddler [17] further leverage heterogeneous CPU-GPU execution. However, these systems mainly optimize expert movement under a given routing pattern and are largely evaluated on text-centric workloads, without explicitly exploiting the routing characteristics introduced by visual tokens. *In contrast, VisMMOE is complementary to this line of work: it improves the effectiveness of expert caching and prefetching in visual-heavy VL-MoE settings by making expert demand itself more compact and predictable.*

## 6 Conclusion

In this work, we present *VisMMOE*, a system for efficient inference of large-scale vision-language MoE models on memory-constrained single-GPU platforms. Our central insight is that visual token compression can be used not only to reduce visual processing cost, but also to compact the expert working set and improve expert predictability during offloaded inference. Guided by this observation, *VisMMOE* reduces the latency and bandwidth overhead of dynamic expert loading through the co-design of compression, prediction, and runtime scheduling. We implement and validate *VisMMOE* on top of multiple software backends. More broadly, our results suggest that co-optimizing model inputs and system execution is a promising direction for practical VL-MoE deployment under tight memory budgets.

## References

- [1] Saeed Ranjbar Alvar, Gursimran Singh, Mohammad Akbari, and Yong Zhang. 2025. DivPrune: Diversity-based Visual Token Pruning for Large Multimodal Models. arXiv:2503.02175 [cs.CV] <https://arxiv.org/abs/2503.02175>
- [2] Reza Yazdani Aminabadi, Samyam Rajbhandari, Ammar Ahmad Awan, Cheng Li, Du Li, Elton Zheng, Olatunji Ruwase, Shaden Smith, Minjia Zhang, Jeff Rasley, and Yuxiong He. 2022. DeepSpeed-inference: enabling efficient inference of transformer models at unprecedented scale. In *Proceedings of the International Conference on High Performance Computing, Networking, Storage and Analysis (Dallas, Texas) (SC '22)*. IEEE Press, Article 46, 15 pages.
- [3] Shuai Bai, Yuxuan Cai, Ruizhe Chen, Keqin Chen, Xionghui Chen, Zesen Cheng, Lianghao Deng, Wei Ding, Chang Gao, Chunjiang Ge, Wenbin Ge, Zhifang Guo, Qidong Huang, Jie Huang, Fei Huang, Binyuan Hui, Shutong Jiang, Zhaohai Li, Mingsheng Li, Mei Li, Kaixin Li, Zicheng Lin, Junyang Lin, Xuejing Liu, Jiawei Liu, Chenglong Liu, Yang Liu, Dayiheng Liu, Shixuan Liu, Dunjie Lu, Ruilin Luo, Chenxu Lv, Rui Men, Lingchen Meng, Xuancheng Ren, Xingzhang Ren, Sibao Song, Yuchong Sun, Jun Tang, Jianhong Tu, Jianqiang Wan, Peng Wang, Pengfei Wang, Qiuyue Wang, Yuxuan Wang, Tianbao Xie, Yiheng Xu, Haiyang Xu, Jin Xu, Zhibo Yang, Mingkun Yang, Jianxin Yang, An Yang, Bowen Yu, Fei Zhang, Hang Zhang, Xi Zhang, Bo Zheng, Humen Zhong, Jingren Zhou, Fan Zhou, Jing Zhou, Yuanzhi Zhu, and Ke Zhu. 2025. Qwen3-VL Technical Report. *arXiv preprint arXiv:2511.21631* (2025).
- [4] Hongtao Chen, Weiyu Xie, Boxin Zhang, Jingqi Tang, Jiahao Wang, Jianwei Dong, Shaoyuan Chen, Ziwei Yuan, Chen Lin, Chengyu Qiu, Yuening Zhu, Qingliang Ou, Jiaqi Liao, Xianglin Chen, Zhiyuan Ai, Yongwei Wu, and Mingxing Zhang. 2025. KTransformers: Unleashing the Full Potential of CPU/GPU Hybrid Inference for MoE Models. In *Proceedings of the ACM SIGOPS 31st Symposium on Operating Systems Principles*.
- [5] Mohamed Dhouib, Davide Buscaldi, Sonia Vanier, and Aymen Shabou. 2025. PACT: Pruning and Clustering-Based Token Reduction for Faster Visual Language Models. In *CVPR*. 14582–14592. doi:10.1109/CVPR52734.2025.01359
- [6] Haojie Duanmu, Xiuhong Li, Zhihang Yuan, Size Zheng, Jiangfei Duan, Xingcheng Zhang, and Dahua Li. 2025. MxMoE: Mixed-precision Quantization for MoE with Accuracy and Performance Co-Design. arXiv:2505.05799 [cs.LG] <https://arxiv.org/abs/2505.05799>
- [7] Artyom Eliseev and Denis Mazur. 2023. Fast Inference of Mixture-of-Experts Language Models with Offloading. arXiv:2312.17238 [cs.LG] <https://arxiv.org/abs/2312.17238>
- [8] Zehao Fan, Zhenyu Liu, Yunzhen Liu, Yayue Hou, Hadjer Benmeziane, Kaoutar El Maghraoui, and Liu Liu. 2025. Context-Aware Mixture-of-Experts Inference on CXL-Enabled GPU-NDP Systems. arXiv:2512.04476 [cs.LG] <https://arxiv.org/abs/2512.04476>
- [9] Othmane Friha, Mohamed Amine Ferrag, Burak Kantarci, Burak Cakmak, Arda Ozgun, and Nassira Ghoulami-Zine. 2024. LLM-Based Edge Intelligence: A Comprehensive Survey on Architectures, Applications, Security and Trustworthiness. *IEEE Open Journal of the Communications Society* 5 (2024), 5799–5856. doi:10.1109/OJCOMS.2024.3456549
- [10] Chaoyou Fu, Peixian Chen, Yunhang Shen, Yulei Qin, Mengdan Zhang, Xu Lin, Jinrui Yang, Xiawu Zheng, Ke Li, Xing Sun, Yunsheng Wu, Rongrong Ji, Caifeng Shan, and Ran He. 2025. MME: A Comprehensive Evaluation Benchmark for Multimodal Large Language Models. arXiv:2306.13394 [cs.CV] <https://arxiv.org/abs/2306.13394>
- [11] Georgi Gerganov. 2023. llama.cpp: Port of Facebook's LLaMA model in C/C++. <https://github.com/ggerganov/llama.cpp>.
- [12] Sylvain Gugger, Lysandre Debut, Thomas Wolf, Philipp Schmid, Zachary Mueller, Sourab Mangrulkar, Marc Sun, and Benjamin Bossan. 2022. Accelerate: Training and inference at scale made simple, efficient and adaptable. <https://github.com/huggingface/accelerate>.
- [13] Duc Hoang, Ajay Jaiswal, Mohammad Samragh, and Minsik Cho. 2026. SpecMD: A Comprehensive Study On Speculative Expert Prefetching. arXiv:2602.03921 [cs.LG] <https://arxiv.org/abs/2602.03921>
- [14] Yushi Huang, Zining Wang, Zhihang Yuan, Yifu Ding, Ruihao Gong, Jinyang Guo, Xianglong Liu, and Jun Zhang. 2026. MoDES: Accelerating Mixture-of-Experts Multimodal Large Language Models via Dynamic Expert Skipping. arXiv:2511.15690 [cs.CV] <https://arxiv.org/abs/2511.15690>
- [15] Ahmadreza Jeddi, Negin Baghbanzadeh, Elham Dolatabadi, and Babak Taati. 2025. Similarity-Aware Token Pruning: Your VLM but Faster. arXiv:2503.11549 [cs.CV] <https://arxiv.org/abs/2503.11549>
- [16] Albert Q. Jiang, Alexandre Sablayrolles, Antoine Roux, Arthur Mensch, Blanche Savary, Chris Bamford, Devendra Singh Chaplot, Diego de las Casas, Emma Bou Hanna, Florian Bressand, Gianna Lengyel, Guillaume Bour, Guillaume Lample, Léo Renard Lavaud, Lucile Saulnier, Marie-Anne Lachaux, Pierre Stock, Sandeep Subramanian, Sophia Yang, Szymon Antoniak, Teven Le Scao, Théophile Gervet, Thibaut Lavril,

- Thomas Wang, Timothée Lacroix, and William El Sayed. 2024. Mixtral of Experts. arXiv:2401.04088 [cs.LG] <https://arxiv.org/abs/2401.04088>
- [17] Keisuke Kamahori, Tian Tang, Yile Gu, Kan Zhu, and Baris Kasikci. 2025. Fiddler: CPU-GPU Orchestration for Fast Inference of Mixture-of-Experts Models. arXiv:2402.07033 [cs.LG] <https://arxiv.org/abs/2402.07033>
- [18] Rui Kong, Yuanchun Li, Qingtian Feng, Weijun Wang, Xiaozhou Ye, Ye Ouyang, Linghe Kong, and Yunxin Liu. 2024. SwapMoE: Serving Off-the-shelf MoE-based Large Language Models with Tunable Memory Budget. arXiv:2308.15030 [cs.AI] <https://arxiv.org/abs/2308.15030>
- [19] Woosuk Kwon, Zhuohan Li, Siyuan Zhuang, Ying Sheng, Lianmin Zheng, Cody Hao Yu, Joseph E. Gonzalez, Hao Zhang, and Ion Stoica. 2023. Efficient Memory Management for Large Language Model Serving with PagedAttention. In *Proceedings of the ACM SIGOPS 29th Symposium on Operating Systems Principles*.
- [20] Donghyun Lee, Je-Yong Lee, Genghan Zhang, Mo Tiwari, and Azalia Mirhoseini. 2024. CATS: Contextually-Aware Thresholding for Sparsity in Large Language Models. arXiv:2404.08763 [cs.LG] <https://arxiv.org/abs/2404.08763>
- [21] Shuhuai Li, Jianghao Lin, Dongdong Ge, and Yinyu Ye. 2026. MoE-SpAc: Efficient MoE Inference Based on Speculative Activation Utility in Heterogeneous Edge Scenarios. arXiv:2603.09983 [cs.LG] <https://arxiv.org/abs/2603.09983>
- [22] Xinhao Li, Yi Wang, Jiashuo Yu, Xiangyu Zeng, Yuhan Zhu, Haiyan Huang, Jianfei Gao, Kunchang Li, Yanan He, Chenting Wang, Yu Qiao, Yali Wang, and Limin Wang. 2024. VideoChat-Flash: Hierarchical Compression for Long-Context Video Modeling. *arXiv preprint arXiv:2501.00574* (2024).
- [23] Yifan Li, Yifan Du, Kun Zhou, Jinpeng Wang, Wayne Xin Zhao, and Ji-Rong Wen. 2023. Evaluating Object Hallucination in Large Vision-Language Models. In *The 2023 Conference on Empirical Methods in Natural Language Processing*. <https://openreview.net/forum?id=xozjw0kZXF>
- [24] Jingcong Liang, Siyuan Wang, Miren Tian, Yitong Li, Duyu Tang, and Zhongyu Wei. 2026. Not All Models Suit Expert Offloading: On Local Routing Consistency of Mixture-of-Expert Models. arXiv:2505.16056 [cs.LG] <https://arxiv.org/abs/2505.16056>
- [25] Bin Lin, Zhenyu Tang, Yang Ye, Jinfa Huang, Junwu Zhang, Yatian Pang, Peng Jin, Munan Ning, Jiebo Luo, and Li Yuan. 2024. MoE-LLaVA: Mixture of Experts for Large Vision-Language Models. arXiv:2401.15947 [cs.CV] <https://arxiv.org/abs/2401.15947>
- [26] Jizhihui Liu, Feiyi Du, Guangdao Zhu, Niu Lian, Jun Li, and Bin Chen. 2025. HiPrune: Training-Free Visual Token Pruning via Hierarchical Attention in Vision-Language Models. arXiv:2508.00553 [cs.CV] <https://arxiv.org/abs/2508.00553>
- [27] Yuan Liu, Haodong Duan, Yuanhan Zhang, Bo Li, Songyang Zhang, Wangbo Zhao, Yike Yuan, Jiaqi Wang, Conghui He, Ziwei Liu, Kai Chen, and Dahua Lin. 2024. MMBench: Is Your Multi-modal Model an All-around Player? arXiv:2307.06281 [cs.CV] <https://arxiv.org/abs/2307.06281>
- [28] Yuliang Liu, Zhang Li, Mingxin Huang, Biao Yang, Wenwen Yu, Chunyuan Li, Xu-Cheng Yin, Cheng-Lin Liu, Lianwen Jin, and Xiang Bai. 2024. OCRBench: on the hidden mystery of OCR in large multi-modal models. *Science China Information Sciences* 67, 12 (Dec. 2024). doi:10.1007/s11432-024-4235-6
- [29] Zichang Liu, Jue Wang, Tri Dao, Tianyi Zhou, Binhang Yuan, Zhao Song, Anshumali Shrivastava, Ce Zhang, Yuandong Tian, Christopher Re, and Beidi Chen. 2023. Deja Vu: Contextual Sparsity for Efficient LLMs at Inference Time. arXiv:2310.17157 [cs.LG] <https://arxiv.org/abs/2310.17157>
- [30] NVIDIA Corporation. 2020. NVIDIA A100 Tensor Core GPU. <https://www.nvidia.com/en-us/data-center/a100/>. Accessed: 2026-03-04.
- [31] NVIDIA Corporation. 2024. NVIDIA Jetson Orin Architecture. <https://www.nvidia.com/en-us/autonomous-machines/embedded-systems/jetson-orin/>. Accessed: 2026-03-04.
- [32] Tianfan Peng, Yuntao Du, Pengzhou Ji, Shijie Dong, Kailin Jiang, Mingchuan Ma, Yijun Tian, Jinhe Bi, Qian Li, Wei Du, Feng Xiao, and Lizhen Cui. 2025. Can Visual Input Be Compressed? A Visual Token Compression Benchmark for Large Multimodal Models. arXiv:2511.02650 [cs.CV] <https://arxiv.org/abs/2511.02650>
- [33] Samsung Electronics. 2023. *Samsung NVMe SSD 980 PRO Data Sheet* (rev. 2.1 ed.). Samsung Electronics. [https://download.semiconductor.samsung.com/resources/data-sheet/Samsung-NVMe-SSD-980-PRO-Data-Sheet\\_Rev.2.1\\_230509\\_10129505081019.pdf](https://download.semiconductor.samsung.com/resources/data-sheet/Samsung-NVMe-SSD-980-PRO-Data-Sheet_Rev.2.1_230509_10129505081019.pdf). Accessed: March 2, 2026.
- [34] Noam Shazeer, Azalia Mirhoseini, Krzysztof Maziarz, Andy Davis, Quoc Le, Geoffrey Hinton, and Jeff Dean. 2017. Outrageously Large Neural Networks: The Sparsely-Gated Mixture-of-Experts Layer. arXiv:1701.06538 [cs.LG] <https://arxiv.org/abs/1701.06538>
- [35] Leqi Shen, Guoqiang Gong, Tao He, Yifeng Zhang, Pengzhang Liu, Sicheng Zhao, and Guiguang Ding. 2025. FastVID: Dynamic Density Pruning for Fast Video Large Language Models. arXiv:2503.11187 [cs.CV] <https://arxiv.org/abs/2503.11187>
- [36] Zixu Shen, Kexin Chu, Yifan Zhang, Dawei Xiang, Runxin Wu, and Wei Zhang. 2025. ExpertFlow: Adaptive Expert Scheduling and Memory Coordination for Efficient MoE Inference. arXiv:2510.26730 [cs.DC] <https://arxiv.org/abs/2510.26730>
- [37] Xiaoni Song, Zihang Zhong, Rong Chen, and Haibo Chen. 2025. ProMoE: Fast MoE-based LLM Serving using Proactive Caching. arXiv:2410.22134 [cs.DC] <https://arxiv.org/abs/2410.22134>
- [38] Yixin Song, Zeyu Mi, Haotong Xie, and Haibo Chen. 2024. PowerInfer: Fast Large Language Model Serving with a Consumer-grade GPU. In *Proceedings of the ACM SIGOPS 30th Symposium on Operating Systems Principles (Austin, TX, USA) (SOSP '24)*. Association for Computing Machinery, New York, NY, USA, 590–606. doi:10.1145/3694715.3695964
- [39] Boyuan Sun, Jiaying Zhao, Xihan Wei, and Qibin Hou. 2025. LLaVA-Scissor: Token Compression with Semantic Connected Components for Video LLMs. *arXiv preprint arXiv:2506.21862* (2025).
- [40] Peng Tang, Jiacheng Liu, Xiaofeng Hou, Yifei Pu, Jing Wang, Peng-Ann Heng, Chao Li, and Minyi Guo. 2024. HOBBIT: A Mixed Precision Expert Offloading System for Fast MoE Inference. arXiv:2411.01433 [cs.LG] <https://arxiv.org/abs/2411.01433>
- [41] Jiayang Wu, Wensheng Gan, Zefeng Chen, Shicheng Wan, and Philip S. Yu. 2023. Multimodal Large Language Models: A Survey. arXiv:2311.13165 [cs.AI] <https://arxiv.org/abs/2311.13165>
- [42] Zhiyu Wu, Xiaokang Chen, Zizheng Pan, Xingchao Liu, Wen Liu, Damai Dai, Huazuo Gao, Yiyang Ma, Chengyue Wu, Bingxuan Wang, Zhenda Xie, Yu Wu, Kai Hu, Jiawei Wang, Yaofeng Sun, Yukun Li, Yishi Piao, Kang Guan, Aixin Liu, Xin Xie, Yuxiang You, Kai Dong, Xingkai Yu, Haowei Zhang, Liang Zhao, Yisong Wang, and Chong Ruan. 2024. DeepSeek-VL2: Mixture-of-Experts Vision-Language Models for Advanced Multimodal Understanding. arXiv:2412.10302 [cs.CV] <https://arxiv.org/abs/2412.10302>
- [43] Guoyang Xia, Yifeng Ding, Fengfa Li, Lei Ren, Wei Chen, Fangxiang Feng, and Xiaojie Wang. 2025. FastMMoE: Accelerating Multimodal Large Language Models through Dynamic Expert Activation and Routing-Aware Token Pruning. arXiv:2511.17885 [cs.CV] <https://arxiv.org/abs/2511.17885>
- [44] Xinfeng Xia, Jiacheng Liu, Xiaofeng Hou, Peng Tang, Mingxuan Zhang, Wenfeng Wang, and Chao Li. 2025. MoE-Prism: Disentangling Monolithic Experts for Elastic MoE Services via Model-System Co-Designs. arXiv:2510.19366 [cs.CL] <https://arxiv.org/abs/2510.19366>
- [45] Cheng Xu, Xiaofeng Hou, Jiacheng Liu, Chao Li, Tianhao Huang, Xiaozhi Zhu, Mo Niu, Lingyu Sun, Peng Tang, Tongqiao Xu, Kwang-Ting Cheng, and Minyi Guo. 2023. MMBench: Benchmarking End-to-End Multi-modal DNNs and Understanding Their Hardware-Software Implications. In *2023 IEEE International Symposium on Workload Characterization (IISWC)*. 154–166. doi:10.1109/IISWC52945.2023.00014

- [46] Leyang Xue, Yao Fu, Zhan Lu, Luo Mai, and Mahesh Marina. 2025. MoE-Infinity: Efficient MoE Inference on Personal Machines with Sparsity-Aware Expert Cache. *arXiv:2401.14361 [cs.LG]* <https://arxiv.org/abs/2401.14361>
- [47] Senqiao Yang, Yukang Chen, Zhuotao Tian, Chengyao Wang, Jingyao Li, Bei Yu, and Jiaya Jia. 2024. VisionZip: Longer is Better but Not Necessary in Vision Language Models. *arXiv preprint arXiv:2412.04467* (2024).
- [48] Hanfei Yu, Xingqi Cui, Hong Zhang, Hao Wang, and Hao Wang. 2025. Taming Latency-Memory Trade-Off in MoE-Based LLM Serving via Fine-Grained Expert Offloading. *arXiv:2502.05370 [cs.LG]* <https://arxiv.org/abs/2502.05370>
- [49] Shaolei Zhang, Qingkai Fang, Zhe Yang, and Yang Feng. 2025. LLaVA-Mini: Efficient Image and Video Large Multimodal Models with One Vision Token. *arXiv:2501.03895 [cs.CV]* <https://arxiv.org/abs/2501.03895>
- [50] Yuning Zhang, Grant Pinkert, Nan Yang, Yanli Li, and Dong Yuan. 2026. DuoServe-MoE: Dual-Phase Expert Prefetch and Caching for LLM Inference QoS Assurance. *arXiv:2509.07379 [cs.DC]* <https://arxiv.org/abs/2509.07379>
- [51] Yushu Zhao, Yubin Qin, Yang Wang, Xiaolong Yang, Huiming Han, Shaojun Wei, Yang Hu, and Shouyi Yin. 2026. MoBiLE: Efficient Mixture-of-Experts Inference on Consumer GPU with Mixture of Big Little Experts. In *2026 31st Asia and South Pacific Design Automation Conference (ASP-DAC)*. 999–1005. doi:10.1109/ASP-DAC66049.2026.11420472
- [52] Lianmin Zheng, Liangsheng Yin, Zhiqiang Xie, Chuyue Sun, Jeff Huang, Cody Hao Yu, Shiyi Cao, Christos Kozyrakis, Ion Stoica, Joseph E. Gonzalez, Clark Barrett, and Ying Sheng. 2024. SGLang: Efficient Execution of Structured Language Model Programs. *arXiv:2312.07104 [cs.AI]* <https://arxiv.org/abs/2312.07104>
- [53] Shuzhang Zhong, Yanfan Sun, Ling Liang, Runsheng Wang, Ru Huang, and Meng Li. 2025. HybriMoE: Hybrid CPU-GPU Scheduling and Cache Management for Efficient MoE Inference. In *2025 62nd ACM/IEEE Design Automation Conference (DAC)*. 1–7. doi:10.1109/DAC63849.2025.11133274
- [54] Jiaying Zhu, Yurui Zhu, Xin Lu, Wenrui Yan, Dong Li, Kunlin Liu, Xueyang Fu, and Zheng-Jun Zha. 2025. VisionSelector: End-to-End Learnable Visual Token Compression for Efficient Multimodal LLMs. *arXiv:2510.16598 [cs.CV]* <https://arxiv.org/abs/2510.16598>